

# *In vivo* reprogramming of circuit connectivity in postmitotic neocortical neurons

Andres De la Rossa<sup>1,4</sup>, Camilla Bellone<sup>1,4</sup>, Bruno Golding<sup>1</sup>, Ilaria Vitali<sup>1</sup>, Jonathan Moss<sup>2</sup>, Nicolas Toni<sup>2</sup>, Christian Lüscher<sup>1,3</sup> & Denis Jabaudon<sup>1,3</sup>

The molecular mechanisms that control how progenitors generate distinct subtypes of neurons, and how undifferentiated neurons acquire their specific identity during corticogenesis, are increasingly understood. However, whether postmitotic neurons can change their identity at late stages of differentiation remains unknown. To study this question, we developed an electrochemical *in vivo* gene delivery method to rapidly manipulate gene expression specifically in postmitotic neurons. Using this approach, we found that the molecular identity, morphology, physiology and functional input-output connectivity of layer 4 mouse spiny neurons could be specifically reprogrammed during the first postnatal week by ectopic expression of the layer 5B output neuron-specific transcription factor *Fezf2*. These findings reveal a high degree of plasticity in the identity of postmitotic neocortical neurons and provide a proof of principle for postnatal re-engineering of specific neural microcircuits *in vivo*.

A hallmark of the cerebral cortex is the broad diversity of neuron subtypes that assemble to form local columnar microcircuits<sup>1–4</sup>. Sensory input to these circuits is provided by thalamocortical axons, which target layer 4 spiny neurons (L4 neurons)<sup>5</sup>, whereas motor output is generated by layer 5B (L5B) pyramidal neurons with long-range subcortical projections to the hindbrain and spinal cord (corticobulbar and corticospinal neurons)<sup>6</sup>. During early corticogenesis, specific genetic programs function in ventricular zone progenitors to control the sequential generation of distinct neuronal subtypes, and manipulation of gene expression in these mitotic cells can specifically modify the subtype identities of their progeny<sup>7–10</sup>. After birth, manipulating sensory input<sup>11</sup> or lesioning peripheral<sup>12</sup> or central pathways<sup>13</sup> strongly affects neuronal connectivity during critical periods of circuit maturation<sup>14</sup>. Moreover, postmitotic neurons have the ability to functionally integrate into existing circuits following transplantation into adult networks<sup>15,16</sup>. This postnatal plasticity indicates that, even long after they are born, neurons are not fully committed to specific circuits. On the contrary, additional neurons can be integrated and new connections can be formed in pre-existing networks.

Although the molecular programs that control the generation and differentiation of the distinct neuronal subtypes that form cortical circuits are increasingly understood<sup>17</sup>, it is not known whether these neurons, once they have reached late stages of differentiation, can be reprogrammed *in vivo* to acquire a distinct cell identity; that is, develop the specific molecular, morphological and physiological features of a distinct neuronal subtype. A major hurdle in investigating such late-stage plasticity has been the inability to rapidly and efficiently manipulate gene expression in specific subtypes of postmitotic neurons. Classical electroporation is largely restricted to mitotic cells<sup>18</sup>, whereas infection with viral vectors requires several days for the transgene to be

expressed<sup>19</sup>, and both techniques have relatively low spatial precision. To circumvent these limitations and examine the plasticity of cell-type identity in postmitotic neurons, we devised a nonviral electrochemical approach to manipulate gene expression specifically in postmitotic neurons, which we termed iontoporation (iPo).

We used iPo to selectively modify gene expression in L4 neurons of the primary somatosensory cortex. In contrast with the other excitatory neurons of the neocortex, which are pyramidal projection neurons, L4 neurons are excitatory interneurons with a mostly stellate morphology; they are the main recipients of thalamocortical input and make strictly local projections in a single cortical column<sup>1,20,21</sup>. The transcription factor *Fezf2*, which is necessary and sufficient for cortical progenitors to generate L5B output neurons, is specifically expressed throughout life in L5B neurons<sup>7,8,22</sup>; thus, we examined whether postnatal iontoporation of *Fezf2* into L4 neurons postnatally would reprogram their identity. Using a combination of molecular, morphological, electrophysiological, optogenetic and ultrastructural imaging approaches, we found that *Fezf2*<sup>+</sup> L4 neurons were reprogrammed into L5B neurons during the first postnatal week, acquiring their identity-defining features, including their morphological and functional input/output connectivity in intracortical and extracortical circuits. Our findings provide a new approach for investigating the boundaries of neuronal plasticity and reveal a high level of plasticity in the identity of postmitotic neocortical neurons, whose identity and circuit properties can be specifically reprogrammed long after their birth.

## RESULTS

### Iontoporation allows direct gene delivery into postmitotic neurons

Classical electroporation is largely restricted to mitotic cells<sup>18</sup> (Fig. 1a) and is therefore not suited to rapidly manipulating gene expression in

<sup>1</sup>Department of Basic Neurosciences, University of Geneva, Geneva, Switzerland. <sup>2</sup>Department of Fundamental Neurosciences, University of Lausanne, Lausanne, Switzerland. <sup>3</sup>Clinic of Neurology, Geneva University Hospital, Geneva, Switzerland. <sup>4</sup>These authors contributed equally to this work. Correspondence should be addressed to D.J. (denis.jabaudon@unige.ch).

Received 17 September 2012; accepted 6 December 2012; published online 6 January 2013; doi:10.1038/nn.3299

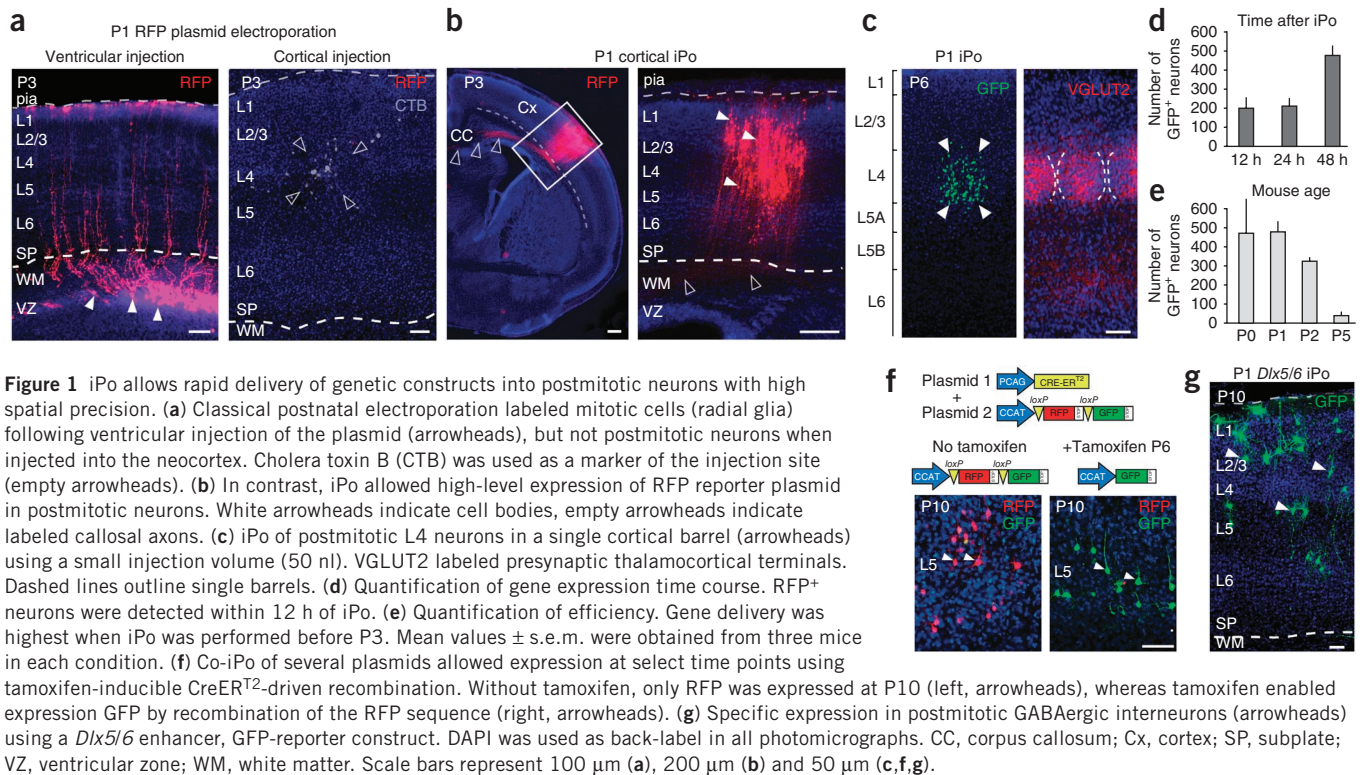


**Figure 1** iPo allows rapid delivery of genetic constructs into postmitotic neurons with high spatial precision. (a) Classical postnatal electroporation labeled mitotic cells (radial glia) following ventricular injection of the plasmid (arrowheads), but not postmitotic neurons when injected into the neocortex. Cholera toxin B (CTB) was used as a marker of the injection site (empty arrowheads). (b) In contrast, iPo allowed high-level expression of RFP reporter plasmid in postmitotic neurons. White arrowheads indicate cell bodies, empty arrowheads indicate labeled callosal axons. (c) iPo of postmitotic L4 neurons in a single cortical barrel (arrowheads) using a small injection volume (50 nl). VGLUT2 labeled presynaptic thalamocortical terminals. Dashed lines outline single barrels. (d) Quantification of gene expression time course. RFP<sup>+</sup> neurons were detected within 12 h of iPo. (e) Quantification of efficiency. Gene delivery was highest when iPo was performed before P3. Mean values  $\pm$  s.e.m. were obtained from three mice in each condition. (f) Co-iPo of several plasmids allowed expression at select time points using tamoxifen-inducible CreER<sup>2</sup>-driven recombination. Without tamoxifen, only RFP was expressed at P10 (left, arrowheads), whereas tamoxifen enabled expression GFP by recombination of the RFP sequence (right, arrowheads). (g) Specific expression in postmitotic GABAergic interneurons (arrowheads) using a *Dlx5/6* enhancer, GFP-reporter construct. DAPI was used as back-label in all photomicrographs. CC, corpus callosum; Cx, cortex; SP, subplate; VZ, ventricular zone; WM, white matter. Scale bars represent 100  $\mu$ m (a), 200  $\mu$ m (b) and 50  $\mu$ m (c,f,g).

select subtypes of neurons in cortical circuits. To circumvent this limitation, we developed a genetic approach to investigate the plasticity of postmitotic neurons in which we stereotactically injected plasmid DNA solubilized in a nuclear permeabilizing agent (trans-cyclohexane-1,2-diol, TCHD)<sup>23</sup> into the somatosensory cortex, and designed a constant-current protocol to deliver the plasmid into neighboring postmitotic neurons. Using iPo, large injection volumes (>200 nl) allowed expression of a reporter gene in neurons in large cortical regions (Fig. 1b), whereas transfection with smaller volumes (<50 nl) was limited to a subset of neurons in a single cortical column (for example, L4; Fig. 1c). Moreover, because of the rapid entry of the plasmid, gene expression was observed in just a few hours (Fig. 1d).

Although the efficiency of iPo with a single plasmid was highest prior to postnatal day 3 (P3; Fig. 1e), co-iPo of multiple plasmids, including an inducible CreER<sup>2</sup> construct<sup>24</sup>, allowed tamoxifen-inducible gene expression into adulthood (Fig. 1f). Furthermore, the use of plasmids with cell subtype-specific promoters (for example, the *Dlx5* and *Dlx6* enhancer element<sup>25</sup> to label GABAergic interneurons; Fig. 1g) enabled neuron subtype-specific expression. Taking advantage of iPo to rapidly manipulate gene expression in select subtypes of neurons, we investigated whether the identity of postmitotic neurons in the somatosensory cortex could be reprogrammed postnatally.

#### Fezf2<sup>+</sup> L4 neurons acquire L5B-like molecular identity

We used iPo to ectopically express the L5B-specific transcription factor *Fezf2* in L4 spiny neurons postnatally, and examined whether this would allow reprogramming of the molecular, morphological, physiological and input/output properties of these neurons to match those of L5B neurons. *Fezf2* is an ideal molecular tool with which to examine these questions, as it is both necessary and sufficient to generate L5B neurons during corticogenesis<sup>7,8,22</sup>. Moreover, the neuronal networks of the primary somatosensory cortex offer an ideal system for studying the temporal boundaries of the postmitotic plasticity in neuron identity:

the distinct neuronal subtypes that compose these circuits and their synaptic relationships are well characterized (Fig. 2a)<sup>1,2</sup>, allowing the relationship between cell identity and connectivity to be examined.

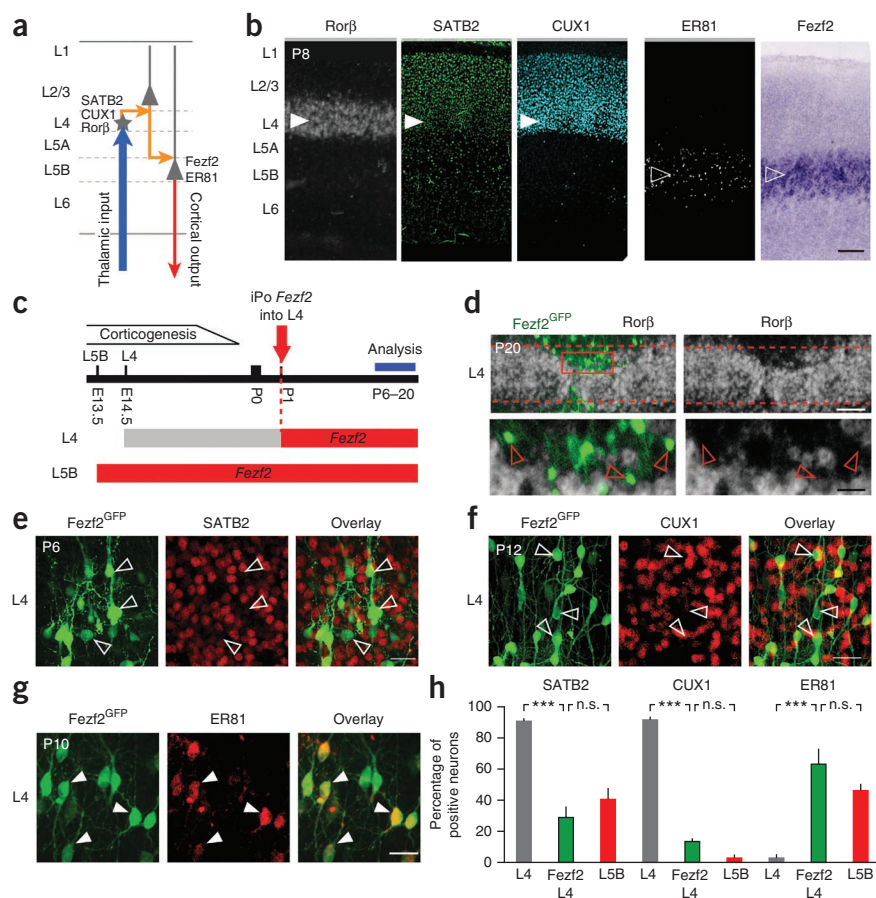
We first characterized the normal molecular identity of L4 neurons using a transgenic mouse line (*Scnn1a-cre*; we refer to these mice as L4Tom)<sup>26</sup> in which we first found that reporter gene expression was specific to L4 spiny neurons (Supplementary Fig. 1a,b). Using this cell type-specific labeling, we were able to define these neurons by the expression of *Rorb*<sup>27,28</sup>, *CUX1* (ref. 29) and *SATB2* (refs. 30,31) (Fig. 2b and Supplementary Fig. 1c–e). In contrast, these genes were not expressed by cortical output neurons in L5B, which instead expressed distinct cell subtype-specific genes, including *Fezf2* (refs. 7,8,22) and *Er81* (also known as *Etv1*)<sup>32</sup> (Fig. 2b).

When *Fezf2* was ectopically expressed in L4 neurons at P1 (Fig. 2c), 7 d after the birth of these neurons, *Rorb*, *SATB2* and *CUX1* expression was repressed, whereas expression of *ER81* was induced (Fig. 2d–h and Supplementary Fig. 2a–d). Notably, genes that were more broadly expressed in several types of cortical output neurons (that is, in both L5B and L6), such as *Ctip2* (also known as *Bcl11b*)<sup>33</sup> and *Sox5* (refs. 34,35), were not induced by *Fezf2* ectopic expression (data not shown), suggesting that the transcriptional programs induced by *Fezf2* expression in L4 are specific to L5B output neurons. Together, these results indicate that postmitotic L4 neurons can be postnatally induced to acquire specific molecular features of L5B output neurons.

#### Fezf2<sup>+</sup> L4 neurons acquire L5B-like neuron morphology

We next examined whether the *Fezf2*-mediated molecular reprogramming was accompanied by L5B output neuron morphology. L4 neurons of the somatosensory cortex mostly have a round soma and stellate morphology with multiple short dendrites that remain confined to L4 (refs. 1,20,21) (Fig. 3a). In contrast, all L5B output neurons are pyramidal with a prominent apical dendrite that reaches L1 (ref. 1) (Fig. 3b). *Fezf2*-iontoporated L4 neurons exhibited a pyramidal soma

**Figure 2** Postnatal expression of *Fezf2* in L4 neurons induces cardinal molecular features of L5B output neurons. **(a)** Schematic representation of the input-output connectivity of a somatosensory barrel column. L4 neurons are the main cortical targets of thalamocortical axons. L5B output neurons specifically expressed *Fezf2* and received only weak thalamocortical input. **(b)** Laminar and cell type-specific gene expression in the neocortex. L4 neurons (white arrowheads) expressed *Rorb*, *SATB2* and *CUX1*, but not *ER81* and *Fezf2*, which are specifically expressed by L5B output neurons (empty arrowheads). **(c)** Summary of the experimental design. *Fezf2* was iontoporated into L4 neurons at P1 and analyses were performed between P6 and P20. **(d–g)** Ectopic expression of *Fezf2* in L4 neurons at P1 repressed *Rorb*, *SATB2* and *CUX1* expression (empty arrowheads) and induced the expression of *ER81* (full arrowheads). **(h)** Quantification of molecular changes for *SATB2*, *CUX1* and *ER81*. Data are presented as mean percentage values  $\pm$  s.e.m. (\*\* $P < 0.001$ , Fisher's exact test,  $n \geq 330$  neurons for each gene). n.s., not significant ( $P > 0.05$ ). Scale bars represent 100  $\mu$ m **(b)** and 25  $\mu$ m **(d–g)**.



and an apical dendrite extending above L4 into superficial layers, reaching the pia and extending tangentially in L1 (neurons with apical dendrite: control L4 neurons,  $17.3 \pm 5.2\%$ ; *Fezf2*<sup>+</sup> L4 neurons,  $81.5 \pm 5.0\%$ ;  $P < 0.001$ , Fisher's exact test; normalized apical dendrite length: L5B neurons,  $1 \pm 0.1$ ; *Fezf2*<sup>+</sup> L4 neurons,  $1.2 \pm 0.1$ ;  $P = 0.2$ , Student's *t* test,  $n = 36$  neurons; **Fig. 3c,d**). Notably, this apical dendrite often bifurcated in L2/3 (**Fig. 3d**), which is typical of L5B output neurons and not of L2/3 projection neurons<sup>1</sup>, suggesting that *Fezf2* induces specific L5B output neuron morphological features rather than a generic pyramidal neuron morphology. The spatial distribution of dendrites using polar distribution analysis was similar in *Fezf2*<sup>+</sup> L4 neurons and L5B output neurons and was distinct from that of control L4 neurons ( $P < 0.001$ , Kolmogorov-Smirnov test for distribution of fractional dendritic length in 10° bins,  $n \geq 13$  neurons per condition; **Fig. 3e**). Moreover, we found that *Fezf2*<sup>+</sup> L4 neurons had fewer basal processes and a less complex dendritic tree than control L4 neurons when examined by Scholl analysis, as found in L5B output neurons, although *Fezf2*<sup>+</sup> L4 neurons tended to have a simpler morphology than L5B neurons, perhaps reflecting a role for *Fezf2* in the stabilization of dendritic processes<sup>8</sup> (Scholl analysis:  $P < 0.001$  for L4 versus *Fezf2*<sup>+</sup> L4 neurons,  $P = 0.09$  for *Fezf2*<sup>+</sup> L4 neurons versus L5B neurons,  $P < 0.05$  if analysis restricted to the first 30  $\mu$ m; Kolmogorov-Smirnov test,  $n \geq 13$  neurons per condition; **Fig. 3f**). Finally, despite their reduced dendritic complexity compared with L4 neurons, the membrane capacitance of *Fezf2*<sup>+</sup> L4 neurons was increased to levels found in L5B neurons, likely reflecting the preponderance of low-resistance large neuronal processes such as the apical dendrite on passive membrane properties (**Fig. 3g**). Together, these results indicate that postmitotic L4 neurons can be postnatally reprogrammed by *Fezf2* to acquire central morphological features of L5B output neurons.

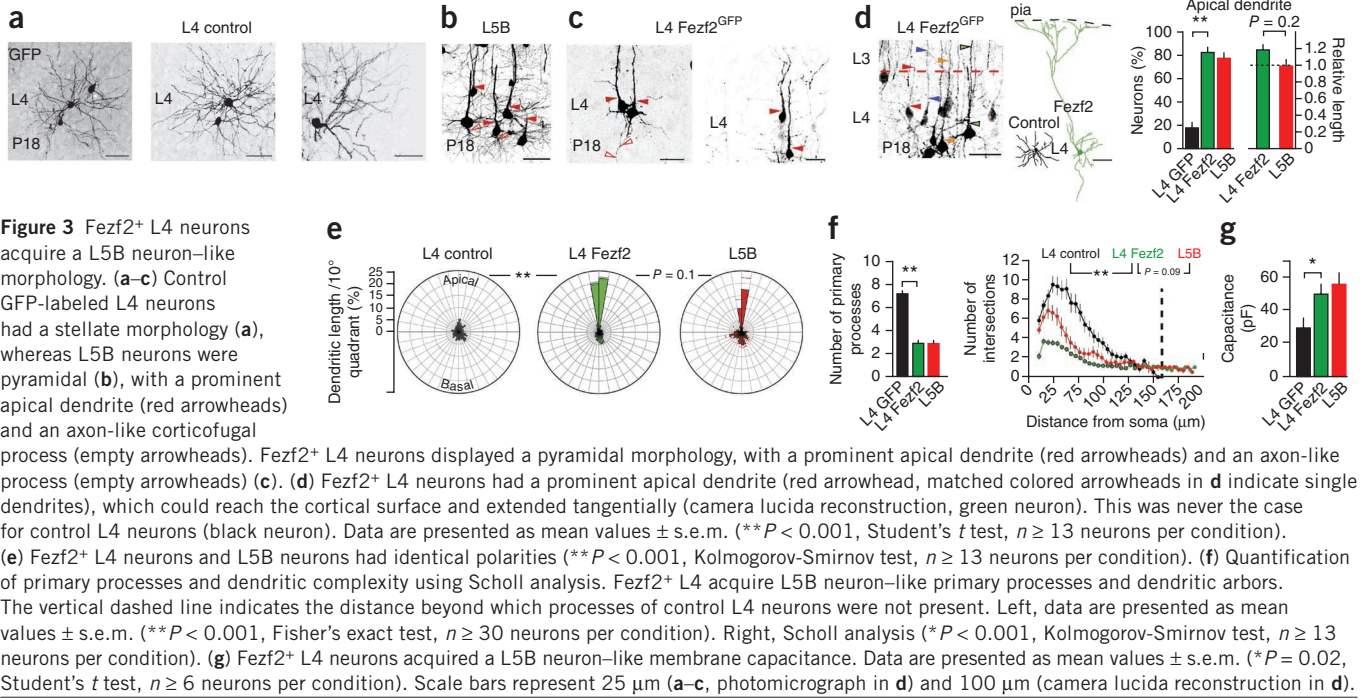
We then tested whether the ability to reprogram L4 neurons into L5B-like output neurons was restricted to a critical period of postnatal development. To this end, we induced ectopic *Fezf2* expression at P10 instead of P1 via iPo of a CreERT<sup>2</sup> tamoxifen-inducible plasmid<sup>24</sup>

(**Supplementary Fig. 3a**). Under these conditions, ectopic expression of *Fezf2* in L4 neurons led to subtle morphological changes, including frequent presence of a prominent apical dendrite (**Supplementary Fig. 3b,c**), but without the overall changes in the genes studied above (**Supplementary Fig. 3d,e**). Together, these findings indicate that, although postmitotic neurons become less amenable to reprogramming with time, select morphological features remain plastic long after the birth of these neurons.

### *Fezf2*<sup>+</sup> L4 neurons acquire L5B-like output properties

We next examined whether, in addition to the specific molecular and morphological reprogramming described above, *Fezf2*<sup>+</sup> L4 neurons acquire the output connectivity and electrophysiological output properties of L5B neurons. L4 neurons make strictly local intracortical connections and their axons do not extend into subcortical structures<sup>1,20,21</sup>. In contrast, L5B output neurons have large-diameter axons that project subcortically through the striatum to the pons and spinal cord<sup>1</sup>. The pyramidal morphology of *Fezf2*<sup>+</sup> L4 neurons, together with the frequent presence of a clearly visible axon-like process in these neurons (**Fig. 3c**), suggested to us that they possessed L5B neuron-like axonal projections. Ankyrin-G immunostaining<sup>36</sup> confirmed that the observed processes were indeed large initial axonal segments (**Fig. 4a**); furthermore, camera lucida reconstructions of *z* stack confocal images revealed that *Fezf2*<sup>+</sup> L4 neurons were able to project outside of the neocortex into subcortical structures (**Fig. 4b**). Confirming these findings, GFP<sup>+</sup> axons extended into the striatum by P20 when *Fezf2*<sup>GFP</sup> (a *Fezf2*-IRES-GFP construct) was iontoporated into L4 neurons at P1, whereas this was not the case when we used a control GFP-expressing plasmid (**Fig. 4c**).

These data suggest that postmitotic L4 neurons can acquire the morphological axonal properties of L5B output neurons following



Fezf2 expression. We next examined whether this morphological reprogramming of Fezf2<sup>+</sup> L4 neuron output was accompanied by a reprogramming of functional output properties. Using whole-cell patch-clamp recording, we found that suprathreshold depolarization of L4 neurons usually evoked a short burst of action potentials (doublet or triplet, interspike interval (ISI) < 40 ms, as previously described<sup>20,37</sup>), whereas L5B neurons had a longer first ISI on average.

Notably, ectopic expression of Fezf2 modified the firing properties of L4 neurons, prolonging the ISI to values found in L5B neurons (*P* < 0.005, Student's *t* test; Fig. 4d). To examine whether the acquisition of L5B-like firing properties reflect broader changes in Fezf2<sup>+</sup> L4 neuron physiology, we used unbiased discriminant analysis based on ten electrophysiological parameters to classify L4, L5B and Fezf2<sup>+</sup> L4 neurons (Table 1 and Supplementary Fig. 4a)<sup>20,38</sup>. This approach

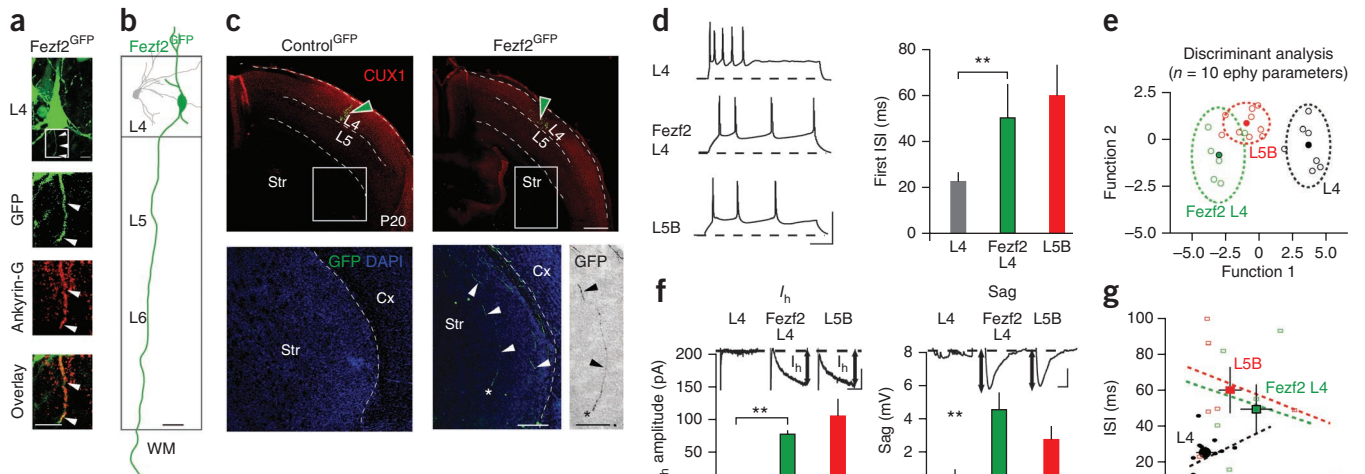


**Figure 4** Fezf2<sup>+</sup> L4 neurons acquire L5B neuron-like output properties.

(a) Ankyrin-G expression identified the initial axonal segment of Fezf2<sup>+</sup> L4 neurons (arrowheads). (b) Camera lucida reconstruction. Fezf2<sup>+</sup> neurons could extend their axon subcortically. (c) Subcortical GFP<sup>+</sup> axonal projections were visible in the striatum of L4 Fezf2<sup>GFP</sup>-iontoporated brains. Inset, high magnification. Green arrowheads indicate the site of iPo. (d) Fezf2 induced L5B neuron-like evoked firing in L4 neurons. Fezf2<sup>+</sup> L4 neurons acquire L5B neuron-like evoked firing activity. Sample traces showing short first ISIs in Fezf2<sup>+</sup> L4 and L5B neurons (mean values ± s.e.m., \*\**P* = 0.005, Student's *t* test, *n* = 27 neurons). (e) Unbiased cluster analysis using ten electrophysiological parameters (Table 1) revealed that Fezf2<sup>+</sup> L4 and L5B neurons have closely related intrinsic electrophysiological properties. (f) Fezf2 induced an H current (*I<sub>h</sub>*) and a sag potential in L4 neurons similar to those of L5B neurons (mean values ± s.e.m., \*\**P* < 0.005, ANOVA, *n* = 21 for *I<sub>h</sub>* and 26 for Sag). Circled numbers indicate number of neurons recorded. (g) First ISI and sag potential values sufficed to parcellate neurons into L4, Fezf2<sup>+</sup> L4 and L5B populations (100% of L4 neurons correctly classified, 50% for Fezf2<sup>+</sup> L4 and L5B neurons). Dashed lines indicate linear regression lines and full symbols indicate average values. Individual cells are represented by the smaller symbols. Scale bars represent 10 μm (a), 50 μm (b), 500 μm (c, top), 250 μm (c bottom) and 100 μm (c bottom, inset). Scale bars in d represent 40 mV, 100 ms. Scale bars in f represent 200 ms, 50pA (*I<sub>h</sub>*), and 4 mV, 100 ms (sag).

**Table 1 Electrophysiological properties of L4, Fezf2<sup>+</sup> L4 and L5B neurons**

Parameter	L4 (4)	Fezf2 <sup>+</sup> L4 (F)	L5B (5)	Ranking
Capacitance (pF)*	30.2 ± 5.8	51.7 ± 5.3	57.7 ± 6.6	4 < 5 = F
Sag (mV)*	0.7 ± 0.3	4.7 ± 1.0	2.9 ± 0.7	4 < 5 < F
First ISI (ms)*	23.2 ± 3.2	49.4 ± 13.7	59.6 ± 12.6	4 < 5 = F
Last ISI (ms)*	56.1 ± 4.2	78.0 ± 41.3	99.7 ± 14.8	4 < F < 5
Amplitude spike 1 (mV)	63.9 ± 6.2	67.4 ± 5.5	76.5 ± 2.3	4 = F = 5
Amplitude spike last (mV)*	44.9 ± 4.7	53.4 ± 7.4	64.0 ± 2.8	4 < F < 5
Duration spike 1 (ms)	1.9 ± 0.1	1.8 ± 0.3	1.8 ± 0.2	4 = F = 5
Duration spike 2 (ms)	3.2 ± 0.5	2.7 ± 0.4	2.5 ± 0.3	4 = F = 5
Spike amplitude decrease (%)*	29.0 ± 4.0	22.0 ± 6.6	16.4 ± 1.8	4 > F > 5
Spike duration increase (%)	72.7 ± 2.0	46.0 ± 5.1	39.7 ± 8.1	4 = F = 5
Amplitude AHP spike 1 (mV)	1.5 ± 0.5	4.1 ± 1.6	2.1 ± 0.6	4 = F = 5
Amplitude AHP spike 2 (mV)*	8.1 ± 1.2	12.3 ± 1.2	12.4 ± 1.1	4 < F = 5

\* $P < 0.05$  between L4 and L5B. AHP, after hyperpolarization. Spike 1 and spike 2 indicate first and second spike elicited after a 200-pA, 500-ms current pulse.

allowed a 100% correct classification of L4 neurons, whereas L5B and Fezf2<sup>+</sup> L4 neurons substantially overlapped (Fig. 4e). Together, these data indicate that Fezf2<sup>+</sup> L4 neurons specifically acquire L5B neuron-like intrinsic electrophysiological properties.

We next sought to investigate the mechanism of this acquisition of L5B-like firing properties, and hypothesized that expression of the hyperpolarization-activated, cyclic nucleotide-gated (HCN) channel-mediated cationic current ( $I_h$ ), which regulates neuronal excitability and is highly enriched in L5B output neurons (Supplementary Fig. 4b)<sup>39</sup>, might be involved in this process. Supporting this possibility, we found that, although control L4 neurons did not express an  $I_h$ , all of the Fezf2<sup>+</sup> L4 neurons did express this current, as was the case for L5B output neurons (0 of 5 L4 neurons, 8 of 8 Fezf2<sup>+</sup> L4 neurons, 8 of 8 L5B neurons,  $I_h$  threshold > 30 pA; Fig. 4f). Confirming these data, we were able to detect a voltage sag in current clamp (Fig. 4f), which was

lacking in control L4 neurons. Notably, when correlating sag amplitude and ISI in single neurons, Fezf2<sup>+</sup> L4 and L5B neurons were identified as belonging to a single neuronal population using discriminant analysis, suggesting that Fezf2 induces a coordinated reprogramming of the electrophysiological properties of L4 neurons (100% of L4 neurons correctly classified, 50% of Fezf2<sup>+</sup> L4 neurons and L5B; Fig. 4g). Together, these results indicate that the morphological and physiological output properties of Fezf2<sup>+</sup> L4 neurons are specifically reprogrammed toward the acquisition of L5B neuron features.

### Fezf2<sup>+</sup> L4 neurons acquire L5B-like subcortical inputs

We next investigated whether this cell-intrinsic reprogramming would be accompanied by a corresponding reassignment of the subcortical and intracortical input connectivity of L4 neurons. During postnatal development of the somatosensory cortex, thalamocortical input is required for the assembly of L4 neurons on the barrel walls and the orientation of their dendrites toward the center of the barrel<sup>12</sup>. We hypothesized that loss of L4 neuron identity in Fezf2<sup>+</sup> L4 neurons would lead to defective thalamocortical innervation of these neurons and, consequently, to the exclusion of their processes and/or cell bodies from barrels. Using specific labeling of L4 neurons in L4Tom mice to identify cortical barrels (Fig. 5a), we observed that control GFP<sup>+</sup> L4 neurons were mostly located in barrels, as previously reported<sup>40</sup>. In contrast, Fezf2<sup>+</sup> L4 neurons were predominantly located in between barrels (Fig. 5b,c), suggesting weak thalamocortical input. We used

**Figure 5** Fezf2<sup>+</sup> L4 neurons acquire L5B-like subcortical inputs. (a) Cortical barrels in L4Tom mice. Left, whole-mount image. Right, a single barrel. (b) Although control GFP<sup>+</sup> L4 neurons are found in barrels (arrowhead), Fezf2<sup>+</sup> L4 neurons were found mostly between barrels (empty arrowheads). (c) Quantification (mean values ± s.e.m., \*\* $P < 0.001$ , Fisher's exact test,  $n = 253$  neurons). (d) Although the dendrites of control GFP<sup>+</sup> L4 neurons were predominantly located in the VGLUT2-rich areas, Fezf2<sup>+</sup> L4 dendritic arbors were mostly confined to the septae between barrels. Shown is a flattened cortex preparation. (e) High-contrast image of the photomicrographs in d. Quantification of VGLUT2-GFP overlap in Fezf2<sup>GFP</sup> neurons and control GFP<sup>+</sup> neurons (mean values ± s.e.m., \*\*\* $P < 0.001$ , Fisher's exact test,  $n = 253$  neurons). (f) mEPSC frequency was decreased in Fezf2<sup>+</sup> L4 neurons to levels found in L5B neurons. Sample traces for mEPSCs recorded from L4, Fezf2<sup>+</sup> L4 and L5B neurons. Bottom left, cumulative distribution plot ( $P < 0.05$ , Kolmogorov-Smirnov test). Bottom right, bar graphs showing mean mEPSC frequency (mean values ± s.e.m., \* $P < 0.05$  between L4 and Fezf2<sup>+</sup> L4 neurons, Student's  $t$  test,  $n = 20$  neurons). (g) Schematic representation of the experimental setup. Sample traces and quantification showing decreased thalamocortical responses in Fezf2<sup>+</sup> L4 neurons (\* $P < 0.01$ , paired  $t$  test;  $n = 5$  pairs of neurons). Cb, cerebellum, Cx, cortex, OB, olfactory bulb, S1, primary somatosensory cortex, n.s.: non significant. Scale bars represent 200  $\mu$ m (a), 50  $\mu$ m (b,e) and 50  $\mu$ m (d). Scale bars in f represent 25 pA, 200 ms, and scale bars in g represent 10 pA, 10 ms.

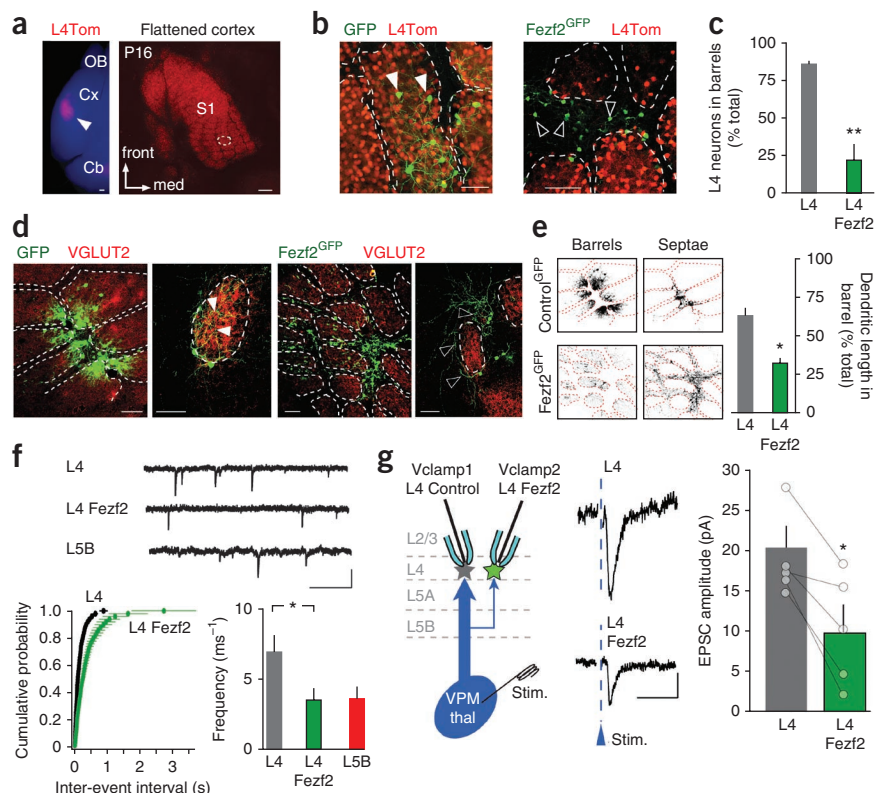
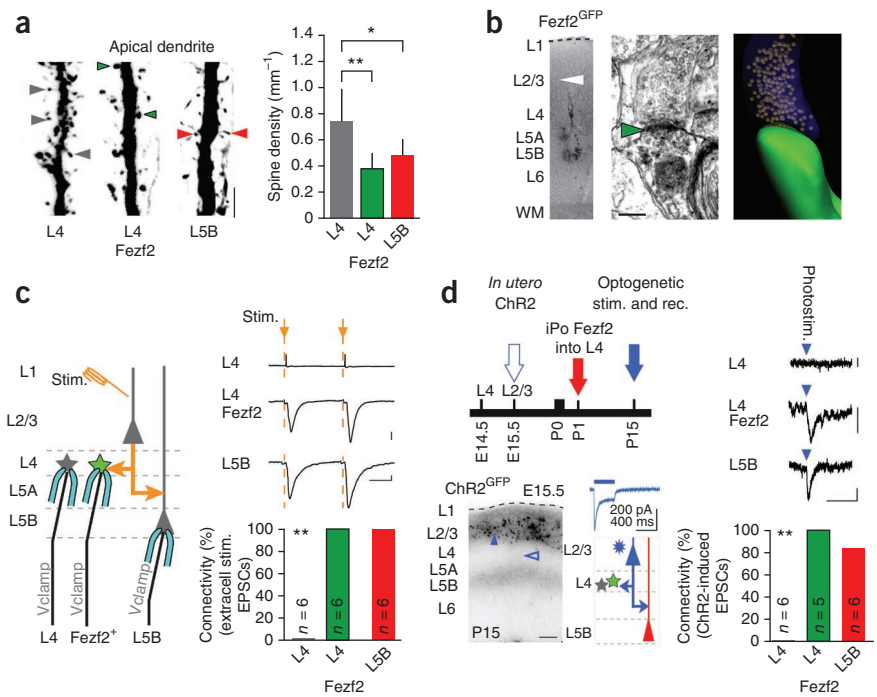


**Figure 6** Fezf2<sup>+</sup> L4 neurons acquire L5B-like intracortical inputs. (a) Spines were present on the apical dendrite of Fezf2<sup>+</sup> L4 neurons at densities similar to those of L5B neurons (mean values  $\pm$  s.e.m., \* $P < 0.05$ , \*\* $P < 0.005$ , Student's *t* test,  $n = 45$  neurons). Scale bar represents 5  $\mu\text{m}$ . (b) Electron micrograph and three-dimensional reconstruction of a synapse on the apical dendrite of a Fezf2<sup>+</sup> L4 neuron, at the level shown in the left panel (white arrowhead). Green arrowhead indicates postsynaptic density of the Fezf2<sup>+</sup> L4 neuron. Scale bar represents 200 nm. (c) Fezf2<sup>+</sup> L4 neurons acquired intracortical input from L2/3. Left, experimental setup. Right, sample traces and connectivity bar graph for results obtained with low-intensity stimulation of L2/3 with an extracellular electrode. Although control L4 neurons did not receive input from L2/3, both Fezf2<sup>+</sup> L4 neurons and L5B neurons did. \*\* $P < 0.005$ , Fisher's exact test. Scale bars represent 50 pA and 20 ms. (d) Fezf2<sup>+</sup> L4 neurons acquired L2/3 neuron input. Top left, experimental setup. Bottom left, ChR2<sup>+</sup> neurons (blue arrowhead) were confined to L2/3 (empty arrowhead, L4). Shown are a summary of the experimental setup and a sample recording of a photocurrent induced by a 400-ms light pulse in a ChR2<sup>+</sup> L2/3 neuron. Right, sample traces and connectivity bar graph for responses evoked in L4, Fezf2<sup>+</sup> L4 and L5B neurons by photostimulation of ChR2-expressing L2/3 neurons. Control L4 neurons did not receive input from L2/3 neurons, whereas both Fezf2<sup>+</sup> L4 neurons and L5B neurons did. \*\* $P < 0.005$ , Fisher's exact test. Scale bars represent 100  $\mu\text{m}$ , 10 pA and 50 ms.



VGLUT2 immunoreactivity to specifically identify the presynaptic terminals of thalamocortical axons<sup>27</sup> (Fig. 5d) and found only a low density of thalamocortical synapses onto the dendrites of Fezf2<sup>+</sup> L4 neurons, which were predominantly located in septae (Fig. 5d,e). Cell death did not detectably contribute to the low proportion of Fezf2<sup>+</sup> L4 neurons in barrels, as observed by the scarcity of caspase3<sup>+</sup> neurons in Fezf2-iontoporated brains at P3 and P6 (Supplementary Fig. 5).

Finally, we examined the functional properties of thalamocortical input onto Fezf2<sup>+</sup> L4 neurons. To assess the overall synaptic input onto these neurons, we recorded miniature excitatory postsynaptic currents (mEPSCs) in acute thalamocortical slices between P10 and P16. We observed a significantly lower frequency of mEPSCs in Fezf2<sup>+</sup> L4 neurons than in control L4 neurons ( $P < 0.05$ ), which was indistinguishable from the mEPSCs frequency observed in L5B neurons (Fig. 5f). Notably, mEPSC amplitude was similar across neuronal subtypes (data not shown), suggesting normal postsynaptic function in Fezf2<sup>+</sup> L4 neurons.

L4 neurons of the somatosensory cortex receive strong input from ventroposterior medial nucleus (VPM) thalamocortical neurons, whereas this input is much weaker in L5B neurons<sup>2,41</sup>. To directly examine whether thalamocortical input was decreased in Fezf2<sup>+</sup> L4 neurons, we selectively stimulated thalamocortical axons while recording from neighboring control L4 and Fezf2<sup>+</sup> L4 neurons. We observed a decrease in functional thalamocortical input onto the Fezf2<sup>+</sup> L4 neurons (Fig. 5g), suggesting acquisition of a L5B-like thalamocortical input. These currents were most likely monosynaptic, as EPSCs had short latencies ( $5.7 \pm 0.77$  ms) and little temporal jitter ( $0.25 \pm 0.05$  ms). Taken together, these results indicate that postmitotic expression of Fezf2 in L4 neurons causes a specific reprogramming of the subcortical input connectivity of Fezf2<sup>+</sup> L4 neurons.

### Fezf2<sup>+</sup> L4 neurons acquire L5B-like intracortical inputs

L5B neurons receive input from L2/3 neurons, yet this input is absent in L4 neurons<sup>2,6</sup>. We examined whether Fezf2 expression could

reprogram the intracortical circuit identity of L4 neurons and induce innervation by L2/3 neurons. Given that the apical dendrite is a major site for L2/3 input in L5B neurons<sup>2</sup>, we first investigated whether we could detect synapses on this process in Fezf2<sup>+</sup> L4 neurons. Using confocal microscopy, we found dendritic spines on the apical dendrite of Fezf2<sup>+</sup> L4 neurons at densities similar to those found in L5B neurons (L4 neurons,  $0.75 \pm 0.05 \mu\text{m}^{-1}$ ; Fezf2<sup>+</sup> L4 neurons,  $0.38 \pm 0.04 \mu\text{m}^{-1}$ ; L5B neurons,  $0.49 \pm 0.05 \mu\text{m}^{-1}$ ;  $n = 41$  neurons,  $P < 0.005$  for L4 versus Fezf2<sup>+</sup> L4,  $P = 0.01$  for L4 versus L5B,  $P = 0.09$  for Fezf2<sup>+</sup> L4 versus L5B, Student's *t* test; Fig. 6a). Using serial-section electron microscopy to directly visualize these presumptive synapses, we found that presynaptic boutons were contacting these dendritic spines, together forming a synapse defined by the presence of at least three vesicles within 50 nm of the presynaptic membrane, facing a postsynaptic density and a synaptic cleft containing electron-dense material (Fig. 6b).

To determine whether there was a functional input from L2/3 neurons onto Fezf2<sup>+</sup> L4 neurons, we used low-intensity extracellular stimulation in L2 while recording from neighboring control L4 and Fezf2<sup>+</sup> L4 neurons (Fig. 6c). Although activation of L2/3 neurons did not elicit responses in control L4 neurons (zero of six neurons), consistent with the anatomy of cortical circuits described above, stimulation elicited a synaptic response in Fezf2<sup>+</sup> L4 neurons (six of six neurons), as was the case for L5B neurons (six of six neurons) (Fig. 6c). Notably, the facilitation of this synaptic response by paired-pulse stimulation was comparable in L5B and Fezf2<sup>+</sup> L4 neurons, suggesting that their input had similar synaptic release properties (paired-pulse ratio L5B,  $1.13 \pm 0.06$ ; Fezf2<sup>+</sup> L4,  $1.39 \pm 0.15$ ;  $P > 0.05$ ). Given that L4 neurons are normally highly interconnected<sup>2</sup>, these evoked synaptic responses could reflect activation of neighboring Fezf2<sup>+</sup> L4 neurons, which would have retained their original connectivity, or nonspecific stimulation of dendrites and fibers of passage. To directly determine whether these responses reflected activation of L2/3 neurons,

we targeted channelrhodopsin 2 (ChR2) expression in L2/3 neurons by *in utero* electroporation at embryonic day 15.5 (E15.5), the time of birth of these neurons, followed by *Fezf2* L4 iPo at P1. We then recorded evoked synaptic responses in control L4 neurons, *Fezf2*<sup>+</sup> L4 neurons and L5B neurons at P15 by stimulating L2/3 neurons with a 10-ms blue laser light pulse (Fig. 6d). Although photostimulation of ChR2-expressing L2/3 neurons evoked synaptic responses in essentially all of the L5B neurons, no response was present in the L4 neurons, as previously reported<sup>42</sup>. In contrast, all of the *Fezf2*<sup>+</sup> L4 neurons responded to photostimulation of L2/3 neurons (Fig. 6d). These data confirm the findings obtained with extracellular stimulation, and indicate that *Fezf2*<sup>+</sup> L4 neurons, similar to L5B neurons, are recognized as genuine functional targets by L2/3 neurons. Together with decreased thalamocortical input and the presence of subcortical projections, this result indicates that *Fezf2* expression in L4 neurons specifically reprograms the input/output connectivity of these neurons toward the acquisition of a L5B-like circuit identity.

## DISCUSSION

Our findings suggest that the identity of postmitotic neurons can be reprogrammed *in vivo* long after they are born; transcriptional programs can be activated in these neurons that fundamentally reassign their morphology, physiological properties and circuit identity in a coordinated and functionally meaningful manner. These findings reveal a high level of functional plasticity in postmitotic neurons and provide a point of entry for studying the mechanisms that control cell identity and circuit plasticity.

In the somatosensory cortex, the ability of *Fezf2* to reprogram L4 neurons was largely limited to the first postnatal week (that is, up to 14 d after the birth of these neurons), as the ectopic expression of this transcription factor led to only limited changes in the morphological identity of L4 neurons at P10 (Supplementary Fig. 1). The molecular mechanisms that initially enable, and later restrict, this postmitotic plasticity are unknown, but they may partially overlap with the mechanisms limiting critical period plasticity in developing sensory systems, including epigenetic regulation of gene expression, as has been reported for ocular dominance plasticity in the visual cortex<sup>43</sup>. Supporting an epigenetic mechanism, promoter methylation is tightly regulated during neuronal differentiation, where it acts to restrict pluripotency<sup>44</sup>. Finally, the reprogramming of cells from distinct lineages into neurons is also generally most efficient when embryonic or neonatal cells are used, suggesting that common mechanisms may be involved across cell lineages<sup>45</sup>.

On a molecular level, *Fezf2* ectopic expression was able to repress the expression of L4 neuron subtype-specific genes (*Rorb*, *Satb2* and *Cux1*) and induce the expression of L5B-specific genes (*Er81*, HCN). Notably, genes that are expressed in broad populations of deep cortical neurons, including *Sox5* (ref. 34) and *Ctip2* (ref. 33), were not upregulated by *Fezf2*. Together, these findings are consistent with the specific role of this transcription factor in controlling the generation of L5B neurons from neocortical progenitors during development<sup>7</sup>.

At the time *Fezf2* is first ectopically expressed (P1), L4 neurons have been reported to possess an apical dendrite, which retracts by P5 in mice<sup>46</sup>. Thus, the presence of an apical dendrite at later developmental stages in *Fezf2*<sup>+</sup> L4 neurons likely reflects a stabilization of this structure by *Fezf2*-induced molecular programs rather than a *de novo* extension of this process. Supporting this possibility, *Fezf2* loss-of-function experiments in cortical progenitors have shown that the dendritic structure of cortical neurons is abnormal<sup>8</sup>. Furthermore, *CUX1*, which we found to be repressed in *Fezf2*<sup>+</sup> L4 neurons, has also been shown to regulate dendritic branching<sup>47</sup>. *Fezf2*<sup>+</sup> L4 neurons also tended to

have a less complex basal dendritic tree than L5B neurons (Fig. 3f), further supporting a role for *Fezf2* in regulating dendritic morphology. Notably, we found that the apical dendrite of *Fezf2*<sup>+</sup> L4 neurons was a functional cellular process that formed spines and received synaptic input (Fig. 6a,b). Given that L2/3→L5B input is focused on the apical dendrite of L5B neurons<sup>2</sup>, spines on the apical dendrite of *Fezf2*<sup>+</sup> L4 neurons may likewise be the site of input from L2/3 neurons. In this context, it is interesting to speculate that the lack of input from L2/3 might contribute to the retraction of the apical dendrite in L4 neurons and its maintenance in L5B neurons. Supporting this possibility, the apical dendrite of L5B neurons is often inverted in the reeler mutant mouse, in which L2/3 neurons are located below L5B<sup>48</sup>.

The reprogramming of the firing properties of *Fezf2*<sup>+</sup> L4 neurons and the acquisition of an H current ( $I_h$ ) are functionally critical. L4 neurons are a predominantly bursting population, able to fire rapidly and to reliably ensure proper temporal coding of thalamocortical sensory information<sup>20,37</sup>. In contrast, L5B neurons integrate input from diverse populations of neurons and regulate the efficacy with which local activity is transferred to downstream subcortical motor circuits in a process that critically depends on  $I_h$  channels<sup>38</sup>. The expression of  $I_h$  and acquisition of L5B neuron-like firing properties indicate that the subcortical axonal elongation in *Fezf2*<sup>+</sup> L4 neurons is not an isolated morphological event, but instead represents the coordinated acquisition of an output neuron identity. More broadly, together with the acquisition of an intracortical input from L2/3 and a pyramidal morphology, these changes indicate a congruous reprogramming of L4 neuronal properties into those of L5B neurons. Supporting this interpretation, the  $I_h$  channel subunit HCN1 is strongly enriched in the distal apical dendrite of pyramidal neurons<sup>49</sup> and its transcript is only weakly expressed by L4 neurons (Developmental Allen Brain Atlas, P14, <http://developingmouse.brain-map.org/>), suggesting that emergence of this current in *Fezf2*<sup>+</sup> L4 neurons is related to preservation of the apical dendrite.

The breadth and coordinated nature of *Fezf2*-induced reprogramming suggests that this transcription factor may normally act as a 'terminal selector' gene for L5B neurons. Such transcription factors are able to control the terminal identity of mature neurons by regulating the expression of ensembles of genes via binding to simple common DNA motifs, together determining the specific identity features defining a neuron, as was recently found in dopaminergic neurons<sup>50</sup>. It will be interesting to examine whether other neuron type-specific transcription factors, such as *SATB2* or *TBR1*, have similar terminal selector-like properties when expressed at late stages in postmitotic neurons.

The change in the identity of L4 neurons is reflected by a marked rearrangement of the morphology of the barrel cortex. Two sequential events are required for morphological barrel formation. First, whisker-specific bundled thalamocortical afferents must form functional synapses onto L4 neurons. Second, L4 neurons must cluster around these afferents. Abnormal afferentation of L4 results in the lack of clustering of L4 neurons (that is, the absence of barrels), whereas postsynaptic clustering of L4 neurons may be abnormal despite normal thalamocortical afferents. Our VGLUT2 immunostaining findings, together with the decreased response to thalamocortical stimulation, suggest that *Fezf2*<sup>+</sup> L4 neurons are not recognized as thalamocortical targets, resulting in a lack of neuronal clustering and barrel formation. Although abnormal cell-cell interactions between *Fezf2*<sup>+</sup> L4 neurons might also contribute to the lack of clustering, the obligatory thalamocortical afferentation prerequisite for barrels to form is lacking.

Finally, it will be important to examine whether postmitotic reprogramming of cell identity may contribute to rewiring during development or after lesions. As neuronal activity during early life can regulate the development of specific neuronal cell types<sup>25</sup>, it is

conceivable that activity-dependent processes may contribute more broadly to cell identity through the dynamic regulation of transcription factor expression. The high temporal and spatial resolution provided by iontoporation is well suited to answering these questions and to investigating the genetic mechanisms that set the boundaries of neuronal plasticity in health and disease.

## METHODS

Methods and any associated references are available in the [online version of the paper](#).

*Note: Supplementary information is available in the [online version of the paper](#).*

## ACKNOWLEDGMENTS

We thank G. Fishell (New York University) for the gift of the Dlx5/6 plasmid, C.L. Cepko (Harvard University) for the pCAGIG\_IRES\_GFP and pCAG\_ERT2-CRE-ERT2 plasmids, and B. Sauer (US National Institutes of Health) for the pBS302\_STOP plasmid, obtained through Addgene. We are thankful to E. Azim and A. Dayer for helpful comments on the manuscript, and to A. Zimmerman and F. Smets for help with the experiments. We thank B. Cerutti for help with the statistical analysis. C.B. is supported by an Ambizione grant from the Swiss National Science Foundation. C.L. is supported by the Swiss National Science Foundation. The Jabaudon laboratory is supported by the Swiss National Science Foundation (PP00P3-123447), the Velux Foundation, the 3R Foundation and the Brain and Behavior Research Foundation. N.T. and J.M. are supported by the Swiss National Science Foundation (PP00A-119026). D.J. and N.T. are supported by a joint Leenaards Foundation for Scientific Research Award.

## AUTHOR CONTRIBUTIONS

D.J. and A.D.I.R. conceived the project and designed the experiments, D.J. and C.B. designed the electrophysiological experiments, and A.D.I.R., C.B., B.G., J.M., N.T. and I.V. performed the experiments. D.J., A.D.I.R., C.B. and C.L. wrote the manuscript.

## COMPETING FINANCIAL INTERESTS

The authors declare no competing financial interests.

Published online at <http://www.nature.com/doi/10.1038/nn.3299>.

Reprints and permissions information is available online at <http://www.nature.com/reprints/index.html>.

- Lefort, S., Tómm, C., Sarria, J.C.F. & Petersen, C.C.H. The excitatory neuronal network of the C2 barrel column in mouse primary somatosensory cortex. *Neuron* **61**, 301–316 (2009).
- Petreaanu, L., Mao, T., Sternson, S.M. & Svoboda, K. The subcellular organization of neocortical excitatory connections. *Nature* **457**, 1142–1145 (2009).
- Brown, S.P. & Hestrin, S. Intracortical circuits of pyramidal neurons reflect their long-range axonal targets. *Nature* **457**, 1133–1136 (2009).
- Yoshimura, Y., Dantzker, J.L.M. & Callaway, E.M. Excitatory cortical neurons form fine-scale functional networks. *Nature* **433**, 868–873 (2005).
- Schubert, D., Kötter, R. & Staiger, J.F. Mapping functional connectivity in barrel-related columns reveals layer- and cell type-specific microcircuits. *Brain Struct. Funct.* **212**, 107–119 (2007).
- Molnár, Z. & Cheung, A.F.P. Towards the classification of subpopulations of layer V pyramidal projection neurons. *Neurosci. Res.* **55**, 105–115 (2006).
- Molyneaux, B.J., Arlotta, P., Hirata, T., Hibi, M. & Macklis, J.D. Fezl is required for the birth and specification of corticospinal motor neurons. *Neuron* **47**, 817–831 (2005).
- Chen, J.-G., Rasin, M.-R., Kwan, K.Y. & Sestan, N. Zfp312 is required for subcortical axonal projections and dendritic morphology of deep-layer pyramidal neurons of the cerebral cortex. *Proc. Natl. Acad. Sci. USA* **102**, 17792–17797 (2005).
- Han, W. *et al.* TBR1 directly represses Fezf2 to control the laminar origin and development of the corticospinal tract. *Proc. Natl. Acad. Sci. USA* **108**, 3041–3046 (2011).
- Weimann, J.M. *et al.* Cortical neurons require Otx1 for the refinement of exuberant axonal projections to subcortical targets. *Neuron* **24**, 819–831 (1999).
- Sperry, R. Effect of 180 degree rotation of the retinal field on visuomotor coordination. *J. Exp. Zool.* **92**, 263–279 (1943).
- Van der Loos, H. & Woolsey, T.A. Somatosensory cortex: structural alterations following early injury to sense organs. *Science* **179**, 395–398 (1973).
- Sur, M., Garraghty, P.E. & Roe, A.W. Experimentally induced visual projections into auditory thalamus and cortex. *Science* **242**, 1437–1441 (1988).
- Hensch, T.K. Critical period plasticity in local cortical circuits. *Nat. Rev. Neurosci.* **6**, 877–888 (2005).
- Martinez-Cerdeño, V. *et al.* Embryonic MGE precursor cells grafted into adult rat striatum integrate and ameliorate motor symptoms in 6-OHDA-lesioned rats. *Cell Stem Cell* **6**, 238–250 (2010).
- Czupryn, A. *et al.* Transplanted hypothalamic neurons restore leptin signaling and ameliorate obesity in db/db mice. *Science* **334**, 1133–1137 (2011).
- Molyneaux, B.J., Arlotta, P., Menezes, J.R.L. & Macklis, J.D. Neuronal subtype specification in the cerebral cortex. *Nat. Rev. Neurosci.* **8**, 427–437 (2007).
- Barnabé-Heider, F. *et al.* Genetic manipulation of adult mouse neurogenic niches by *in vivo* electroporation. *Nat. Methods* **5**, 189–196 (2008).
- Lowery, R.L. *et al.* Rapid, long-term labeling of cells in the developing and adult rodent visual cortex using double-stranded adeno-associated viral vectors. *Dev. Neurobiol.* **69**, 674–688 (2009).
- Staiger, J.F. *et al.* Functional diversity of layer IV spiny neurons in rat somatosensory cortex: quantitative morphology of electrophysiologically characterized and biocytin labeled cells. *Cereb. Cortex* **14**, 690–701 (2004).
- Lübke, J., Egger, V., Sakmann, B. & Feldmeyer, D. Columnar organization of dendrites and axons of single and synaptically coupled excitatory spiny neurons in layer 4 of the rat barrel cortex. *J. Neurosci.* **20**, 5300–5311 (2000).
- Chen, B., Schaevitz, L.R. & McConnell, S.K. Fezl regulates the differentiation and axon targeting of layer 5 subcortical projection neurons in cerebral cortex. *Proc. Natl. Acad. Sci. USA* **102**, 17184–17189 (2005).
- Vandenbroucke, R.E., Lucas, B., Demeester, J., De Smedt, S.C. & Sanders, N.N. Nuclear accumulation of plasmid DNA can be enhanced by non-selective gating of the nuclear pore. *Nucleic Acids Res.* **35**, e86 (2007).
- Matsuda, T. & Cepko, C.L. Controlled expression of transgenes introduced by *in vivo* electroporation. *Proc. Natl. Acad. Sci. USA* **104**, 1027–1032 (2007).
- De Marco Garcia, N.V., Karayannis, T. & Fishell, G. Neuronal activity is required for the development of specific cortical interneuron subtypes. *Nature* **472**, 351–355 (2011).
- Madisen, L. *et al.* A robust and high-throughput Cre reporting and characterization system for the whole mouse brain. *Nat. Neurosci.* **13**, 133–140 (2010).
- Jabaudon, D., Shnyder, S.J., Tischfield, D.J., Galazo, M.J. & Macklis, J.D. RORB induces barrel-like neuronal clusters in the developing neocortex. *Cereb. Cortex* **22**, 996–1006 (2012).
- Nakagawa, Y. & O'Leary, D.D.M. Dynamic patterned expression of orphan nuclear receptor genes RORalpha and RORbeta in developing mouse forebrain. *Dev. Neurosci.* **25**, 234–244 (2003).
- Nieto, M. *et al.* Expression of Cux-1 and Cux-2 in the subventricular zone and upper layers II–IV of the cerebral cortex. *J. Comp. Neurol.* **479**, 168–180 (2004).
- Alcama, E.A. *et al.* Satb2 regulates callosal projection neuron identity in the developing cerebral cortex. *Neuron* **57**, 364–377 (2008).
- Britanova, O. *et al.* Satb2 is a postmitotic determinant for upper-layer neuron specification in the neocortex. *Neuron* **57**, 378–392 (2008).
- Yoneshima, H. *et al.* Er81 is expressed in a subpopulation of layer 5 neurons in rodent and primate neocortices. *Neuroscience* **137**, 401–412 (2006).
- Arlotta, P. *et al.* Neuronal subtype-specific genes that control corticospinal motor neuron development *in vivo*. *Neuron* **45**, 207–221 (2005).
- Lai, T. *et al.* SOX5 controls the sequential generation of distinct corticofugal neuron subtypes. *Neuron* **57**, 232–247 (2008).
- Kwan, K.Y. *et al.* SOX5 postmitotically regulates migration, postmigratory differentiation, and projections of subplate and deep-layer neocortical neurons. *Proc. Natl. Acad. Sci. USA* **105**, 16021–16026 (2008).
- Inda, M.C., DeFelipe, J. & Muñoz, A. Voltage-gated ion channels in the axon initial segment of human cortical pyramidal cells and their relationship with chandelier cells. *Proc. Natl. Acad. Sci. USA* **103**, 2920–2925 (2006).
- Connors, B.W. & Gutnick, M.J. Intrinsic firing patterns of diverse neocortical neurons. *Trends Neurosci.* **13**, 99–104 (1990).
- Andjelic, S. *et al.* Glutamatergic nonpyramidal neurons from neocortical layer VI and their comparison with pyramidal and spiny stellate neurons. *J. Neurophysiol.* **101**, 641–654 (2009).
- Sheets, P.L. *et al.* Corticospinal-specific HCN expression in mouse motor cortex: I<sub>h</sub>-dependent synaptic integration as a candidate microcircuit mechanism involved in motor control. *J. Neurophysiol.* **106**, 2216–2231 (2011).
- Narbox-Nême, N. *et al.* Neurotransmitter release at the thalamocortical synapse instructs barrel formation, but not axon patterning in the somatosensory cortex. *J. Neurosci.* **32**, 6183–6196 (2012).
- Viaene, A.N., Petrof, I. & Sherman, S.M. Synaptic properties of thalamic input to the subgranular layers of primary somatosensory and auditory cortices in the mouse. *J. Neurosci.* **31**, 12738–12747 (2011).
- Petreaanu, L., Huber, D., Sobczyk, A. & Svoboda, K. Channelrhodopsin-2-assisted circuit mapping of long-range callosal projections. *Nat. Neurosci.* **10**, 663–668 (2007).
- Putignano, E. *et al.* Developmental downregulation of histone post-translational modifications regulates visual cortical plasticity. *Neuron* **53**, 747–759 (2007).
- Mohn, F. *et al.* Lineage-specific polycomb targets and *de novo* DNA methylation define restriction and potential of neuronal progenitors. *Mol. Cell* **30**, 755–766 (2008).
- Kim, J., Ambasudhan, R. & Ding, S. Direct lineage reprogramming to neural cells. *Curr. Opin. Neurobiol.* **22**, 778–784 (2012).
- Callaway, E.M. & Borrell, V. Developmental sculpting of dendritic morphology of layer 4 neurons in visual cortex: influence of retinal input. *J. Neurosci.* **31**, 7456–7470 (2011).
- Cubelos, B. *et al.* Cux1 and Cux2 regulate dendritic branching, spine morphology and synapses of the upper layer neurons of the cortex. *Neuron* **66**, 523–535 (2010).
- Terashima, T., Inoue, K., Inoue, Y., Mikoshiba, K. & Tsukada, Y. Distribution and morphology of callosal commissural neurons within the motor cortex of normal and reeler mice. *J. Comp. Neurol.* **232**, 83–98 (1985).
- Lörincz, A., Notomi, T., Tamás, G., Shigemoto, R. & Nusser, Z. Polarized and compartment-dependent distribution of HCN1 in pyramidal cell dendrites. *Nat. Neurosci.* **5**, 1185–1193 (2002).
- Flames, N. & Hobert, O. Gene regulatory logic of dopamine neuron differentiation. *Nature* **458**, 885–889 (2009).

## ONLINE METHODS

**Mouse strains.** CD1 mice (Charles River Laboratory) were iontoporated at P1 unless indicated otherwise. The *Scnn1a-cre* mouse line was obtained from Jackson Laboratories (stock number 009613). Where indicated, tamoxifen was administered intraperitoneally (100  $\mu$ l, 10 mg ml<sup>-1</sup>) at P10. *In utero* electroporation of ChR2 was performed at E15.5 as previously described<sup>27,34</sup>. All of the experiments were carried out in accordance with the Institutional Animal Care and Use Committee of the University of Geneva and with permission of the Geneva cantonal authorities.

**Postnatal iontoporation.** We anesthetized P1 pups on ice for 5 min and placed them on a stereotactic frame. A small skin incision was performed on the skull and 50–200 nl of DNA (5  $\mu$ g  $\mu$ l<sup>-1</sup>) was injected using a 30- $\mu$ m-tip glass micropipette mounted on a nanoject II nanoinjector (Drummond). Prior to injection, the plasmid solution was mixed with 1  $\mu$ l of TCHD (100 mg ml<sup>-1</sup>) to enhance nuclear membrane permeability<sup>23,51</sup>. We placed 5-mm electrode paddles on each side of the skull 4 min after injection and gave two trains of ten pulses (1 Hz, 50-ms duration) using a 50-mA constant-current protocol with an electroporator. After surgery, we kept the pups on a warm plate and placed them back with their mother. Mouse handling was performed in compliance with protocols approved by the Veterinary Office of the Canton of Geneva.

**Plasmids.** We generated plasmids using a standard endotoxin-free Qiagen kit (12362). *Fezf2* cDNA (Open Biosystems clone 6415359) was subcloned into a pCAGIG\_IRES\_GFP (Addgene number 11159) plasmid. The CCAT\_loxp\_RFP\_loxp\_GFP was a gift from G. Elder (Mount Sinai School of Medicine). The pCAGIG\_STOP\_Fezf2\_IRES\_GFP plasmid was made by subcloning the STOP sequence from Addgene plasmid 11925 into pCAGIG\_fezf2\_IRES\_GFP. The pCAG\_ERT2\_CreERT2 plasmid was from Addgene (number 13777). The Dlx5/6 plasmid was a gift from G. Fishell. The Chr2 T159C<sup>52</sup> plasmid was subcloned into the pCAGIG\_IRES\_GFP vector.

**In situ hybridization and immunocytochemistry.** We performed *in situ* hybridization for *Rorb* and *Fezf2* and immunohistochemistry on 50- $\mu$ m tissue sections as previously described<sup>27</sup>. Thicker sections (up to 400  $\mu$ m) were used for camera lucida reconstructions and detection of subcortical axons. For primary antibodies, we used mouse and rabbit antibodies to GFP (1:500, Invitrogen, a11120 and a11122), mouse antibody to SATB2 (1:200, Abcam, ab51502), rabbit antibody to CUX1 (1:500, Santa Cruz, sc-13024), guinea pig antibody to VGLUT2 (1:2,000, Millipore, ab2251), rabbit antibody to ER81 (1:500 Abcam, ab81086), rabbit antibody to Ankyrin-G (1:750, Santa Cruz, sc-28561) and rabbit antibody to Casp3 (1:200, Cell Signaling, 9661).

**Image acquisition, quantification and statistical analysis.** Images were obtained with a Zeiss (LSM 700) confocal microscope and a Nikon 90i microscope and analyzed with Zen software, and reconstructed with NeuroLucida software for neurite analysis.

Analyses were performed between P6 and P20. The molecular identity and barrel cortex cytoarchitecture were assessed at P6 and confirmed at later time points. Electrophysiological analyses were performed between P10–18. Morphological analyses were performed at P18–20.

L4 of the somatosensory cortex was identified by the presence of barrels or the presence of red neurons in L4Tom mice. The percentage of L4 neurons that were positive for CUX1, SATB2 or ER81 immunoreactivity was determined in all sections containing L4 GFP<sup>+</sup> cells and DAPI was used to identify individual cells to count expression frequency in L4 and L5B.

Colabeling of VGLUT2 and GFP was normalized using the equalize function of the Adobe Photoshop CS6 software and quantified using the ImageJ 1.45s histogram/list tool (US National Institutes of Health).

**Electron microscopy.** The samples were processed as previously described<sup>53</sup>. Briefly, mice were perfused transcardially with phosphate-buffered saline,

followed by fixative (4% paraformaldehyde (wt/vol), 1% glutaraldehyde (vol/vol), in 0.1 M phosphate buffer) and 50- $\mu$ m-thick brain sections were immunostained for GFP (rabbit antibody to GFP, 1:1,000, Invitrogen, cat #A11122). Labeled cells were then revealed using a biotinylated secondary antibody (goat antibody to rabbit (F)ab fragment, 1:200, Jackson Laboratories, cat #111-066-047), an avidin-biotin-peroxydase complex (ABC Elite, Vector Labs) and a reaction with 3,3'-diaminobenzidine (Vector Labs) for 4 min. After postfixation in 2.5% glutaraldehyde followed by 1% osmium tetroxide (vol/vol) in 0.1 M phosphate buffer, the sections were dehydrated, embedded in durcupan resin (Sigma), and cells and dendrites of interest were identified. We imaged 60-nm ultrathin serial sections of the selected dendrites at a final magnification of 25,000 $\times$  and performed three-dimensional rendering with Fiji software.

**Electrophysiology.** We prepared thalamocortical slices from P10–18 mouse pups as described previously<sup>54,55</sup>. Slices were cut in cooled artificial cerebrospinal fluid containing 119 mM NaCl, 2.5 mM KCl, 1.3 mM MgCl<sub>2</sub>, 2.5 mM CaCl<sub>2</sub>, 1.0 mM Na<sub>2</sub>HPO<sub>4</sub>, 26.2 mM NaHCO<sub>3</sub> and 11 mM glucose, bubbled with 95% O<sub>2</sub> and 5% CO<sub>2</sub>. Slices were kept at room temperature and were allowed to recover for at least 1 h before recording. Under low magnification, the barrels in L4 could be readily identified, and high-power magnification was used to guide the recording electrode onto visually identified neurons. The internal solution contained 140 mM potassium gluconate, 5 mM KCl, 10 mM HEPES, 0.2 mM EGTA, 2 mM MgCl<sub>2</sub>, 4 mM Na<sub>2</sub>ATP, 0.3 mM Na<sub>2</sub>GTP and 10 mM sodium creatine-phosphate. Currents were amplified (Multiclamp 700B, Axon Instruments), filtered at 5 kHz and digitized at 20 kHz (National Instruments Board PCI-MIO-16E4, Igor, WaveMetrics). The liquid junction potential was +12 mV.

Voltage sag was measured in current clamp from resting membrane potential by presenting a hyperpolarizing current step (–100 pA, 500 ms) and was calculated by the difference between peak voltage and steady-state voltage.  $I_h$  was measured in voltage clamp using a –40-mV step (500 ms) and was calculated by the difference between the peak current and steady-state current. No synaptic blockers were present during these recordings. Cells were voltage clamped at –60 mV and thalamocortical EPSCs were evoked at a frequency of 0.1 Hz by a bipolar stimulating electrode placed in the VB nucleus. The lowest intensity evoking a response was used to avoid activation of corticothalamic fibers and other passing fibers. For intracortical stimulation, the stimulating electrode was placed in superficial layer 2 and the lowest intensity evoking a response was used. Photostimulation was performed using 10-ms blue laser light pulses every 30 s in L2/3 ChR2-expressing sections<sup>42</sup>, and photo-induced EPSCs were recorded from L4, L5B or *Fezf2*<sup>+</sup> L4 neurons. mEPSCs were recorded in the presence of tetrodotoxin (0.5  $\mu$ M). The frequency and amplitude properties of these currents were then analyzed using the Mini Analysis software package (v.4.3, Synaptosoft). Changes in cumulative miniature EPSC amplitude and inter-event interval distribution were analyzed for statistical significance using the nonparametric two-sample Kolmogorov-Smirnov test (KyPlot) with a conservative critical probability level of  $P < 0.05$ .

**Statistical analysis.** We used Student's two-sided  $t$  test for parametric data and Fisher's exact test for non-parametric data, and Kolmogorov-Smirnov test for comparison of distributions, unless stated otherwise.

- Liashkovich, I., Meyring, A., Kramer, A. & Shahin, V. Exceptional structural and mechanical flexibility of the nuclear pore complex. *J. Cell. Physiol.* **226**, 675–682 (2011).
- Berndt, A. *et al.* High-efficiency channelrhodopsins for fast neuronal stimulation at low light levels. *Proc. Natl. Acad. Sci. USA* **108**, 7595–7600 (2011).
- Toni, N. *et al.* Neurons born in the adult dentate gyrus form functional synapses with target cells. *Nat. Neurosci.* **11**, 901–907 (2008).
- Bannister, N.J. *et al.* Developmental changes in AMPA and kainate receptor-mediated quantal transmission at thalamocortical synapses in the barrel cortex. *J. Neurosci.* **25**, 5259–5271 (2005).
- Daw, M.I., Bannister, N.V. & Isaac, J.T. Rapid, activity-dependent plasticity in timing precision in neonatal barrel cortex. *J. Neurosci.* **26**, 4178–4187 (2006).